Article

Photocatalytic Remediation of Harmful *Alexandrium minutum* Bloom Using Hybrid Chitosan-Modified TiO$_2$ Films in Seawater: A Lab-Based Study

Nur Hanisah Ibrahim [1], Anwar Iqbal [1,*], Normawaty Mohammad-Noor [2,*], Roziawati Mohd Razali [3], Srimala Sreekantan [4], Dede Heri Yuli Yanto [5,6], Abdul Hanif Mahadi [7] and Lee D. Wilson [8,*]

[1] School of Chemical Sciences, Universiti Sains Malaysia, Minden, Gelugor 11800, Penang, Malaysia; nur_hanisah95@yahoo.com

[2] Department of Marine Science, Kulliyyah of Science, International Islamic University Malaysia, Jalan Sultan Ahmad Shah, Bandar Indera Mahkota, Kuantan 25200, Pahang, Malaysia

[3] Fisheries Research Institute, Batu Maung 11960, Penang, Malaysia; roziawatir80@gmail.com

[4] School of Material and Mineral Resources Engineering, Universiti Sains Malaysia, Nibong Tebal 14300, Penang, Malaysia; srimala@usm.my

[5] Research Center for Applied Microbiology, National Research and Innovation Agency (BRIN), Cibinong, Bogor 16911, Indonesia; dede.heri.yuli.yanto@brin.go.id

[6] Research Collaboration Center for Marine Biomaterials, Jatinangor 45360, Indonesia

[7] Centre for Advanced Material and Energy Sciences, Universiti Brunei Darussalam, Jalan Tungku Link, Gadong, Bandar Seri Begawan BE1410, Brunei; hanif.mahadi@ubd.edu.bn

[8] Department of Chemistry, University of Saskatchewan, 110 Science Place, Room 165 Thorvaldson Building, Saskatoon, SK S7N 5C9, Canada

* Correspondence: anwariqbal@usm.my (A.I.); normahwaty@iium.edu.my (N.M.-N.); lee.wilson@usask.ca (L.D.W.)

Abstract: The uncontrolled growth of harmful algal blooms (HABs) can negatively impact the environment and pose threats to human health and aquatic ecosystems. Titanium dioxide (TiO$_2$) is known to be effective in killing harmful algae through flocculation and sedimentation. However, TiO$_2$ in a dispersed form can harm other non-target marine organisms, which has raised concerns by environmentalists and scientists. This research seeks to explore the utility of immobilized titanium oxide as a photocatalyst for mitigation of HABs, where the *Alexandrium minutum* bloom was used as a model system herein. Chitosan was modified with 0.2 wt.% TiO$_2$ (Chi/TiO$_2$ (*x* mL; *x* = 1, 3 and 5 mL) and the corresponding films were prepared via solvent casting method. Scanning electron microscope (SEM) images of the films reveal a highly uneven surface. X-ray diffraction (XRD) analysis indicates the reduction in chitosan crystallinity, where the presence of TiO$_2$ was negligible, in accordance with its dispersion within the chitosan matrix. The photocatalytic mitigation of *A.minutum* was carried out via a physical approach in a laboratory-scale setting. The negative surface charge of the films was observed to repel the negatively charged *A.minutum* causing fluctuation in the removal efficiency (RE). The highest RE (76.1 $\pm$ 13.8%) was obtained when Chi/TiO$_2$ (1 mL) was used at 72 h, where the hydroxyl radicals generated were inferred to contribute to the deactivation of the algae cells by causing oxidative stress. An outcome of this study indicates that such hybrid films have the potential to replace the non-immobilized (dispersed) TiO$_2$ for HAB mitigation. However, further investigation is required to deploy these films for field applications at a larger scale.

Keywords: chitosan film; TiO$_2$ photocatalyst; harmful algal bloom; hydroxyl radicals; oxidative stress; *Alexandrium minutum* species

1. Introduction

Harmful algal blooms (HABs) are a phenomenon caused by the uncontrolled and rapid growth of toxic and harmful algae. HABs can be generated from a wide range of organisms

such as toxic cyanobacteria, phytoplankton, microalgae and benthic algae [1]. The frequent occurrence of HABs is attributed to global warming and the high input of nutrient species that contain nitrogen and phosphorus from industrial sewage, agricultural and aquaculture runoff and discharge into water bodies [2,3]. In addition, natural environmental factors such as temperature, pH, light irradiance and water currents also contribute to the occurrence of HABs [3]. These harmful algal blooms (HABs) generally form in warm and still water, where HABs appear foamy or scummy on the surface of water bodies, which may occur in both fresh and marine water bodies [4]. A single outbreak of HABs can cause millions of dollars in losses to the fisheries industry, mostly fish farms and the tourism industry. Ingestion of contaminated seafood products by humans through skin contact with toxin-contaminated water, or the inhalation of aerosolized toxins, or noxious compounds can be lethal [5].

Mitigation of HABs is the term used to describe the actions taken to deal with an existing or ongoing bloom by taking necessary precautions to reduce its negative impact [6]. Various biological, chemical and physical approaches have been reported to be successful in HAB mitigation. Although effective, most techniques to control HABs have several limitations such as high maintenance cost, short-term effectiveness and the need for repeated treatments [7]. Control technologies for the mitigation of HABs should be more sustainable at a low maintenance cost with long-term effects that should not cause any direct or indirect impact on human life and aquatic ecosystems.

In wastewater remediation, photocatalysis is one of the widely used advanced oxidation processes (AOPs) that utilize photogenerated electron/hole pairs generated by semiconductors when irradiated with light. In turn, the photogenerated electron/hole pairs can react with moisture and dissolved oxygen to generate reactive oxygen species (ROS), which can cause damage to the structure of the algae and degrade its toxins [8]. Various semiconductors such as TiO_2, ZnO, SnO_2, CuO, CdS and Fe_2O_3 have been used as photocatalyst materials to alter the structure and function of algae cells. Baniamerian et al. reported that Fe_2O_3–TiO_2 nanoparticles show a high removal rate of *Chlorella vulgaris* (99.8%) within 24 h under visible light irradiation [9]. The g-C_3N_4/Bi-TiO_2 floating photocatalyst reported by Song et al., 2021 led to the removal of *Microcystis aeruginosa* (99.2%) within a 3 h exposure [10]. On the other hand, Fan et al., 2022 have reported that the $ZnFe_2O_4$/Ag_3PO_4/g-C_3N_4 (ZFO/AP/CN) photocatalyst had a removal efficacy for *M. aeruginosa* (94.31%) and MC-LR (76.92%) under visible light conditions [11].

Chitosan is a biopolymer with antimicrobial activity that contains glucosamine units with a variable level of N-acetylation at C2, where primary and secondary hydroxyl groups at C6 and C3 that can be used for synthetic modification [12,13]. The chitosan/TiO_2-based nanocomposite films have been extensively studied for wastewater treatment. Such types of chitosan (CS) films reveal remarkable adsorption and photocatalysis of organic and inorganic pollutants. Razzaz et al. found that chitosan functionalized with TiO_2 nanoparticles prepared by the entrapment method exhibited better adsorption of Cu(II) and Pb(II), as compared with nanocomposite particles prepared by the coating method [14]. In 2018, Saravanan et al. reported that chitosan-TiO_2 composites showed great degradation efficiency toward methyl orange dye [15]. Zhao et al. reported that Ag_2O/TiO_2-modified CS-based film was able to completely degrade ampicillin and methyl orange within 180 min and 30 min, respectively [16] Abdullah Al Balushi et al. reported that a chitosan-TiO_2 film with 12 layers of coating was able to completely degrade 0.60 ppm of methylene blue (MB) within 120 min of contact [17].

To the best of our knowledge, no reports can be found on the application of chitosan-TiO_2 film as a strategy for the mitigation of HAB. In this study, chitosan-TiO_2 films were developed via a solvent casting method for the mitigation of *Alexandrium minutum* (*A. minutum*), which is a common algae species frequently found in the northeastern coast of peninsular Malaysia [18]. The lab-scale mitigation study reported herein represents a *first example* that combines a physical and chemical approach involving adsorption and pho-

tocatalysis. This study will demonstrate the effectiveness of this photocatalytic approach of HAB mitigation with its feasibility for scalability and sustainability.

2. Results

As outlined in the introduction, a series of chitosan films were prepared that contain an incremental volumetric dosage of 0.2% *w/v* of anatase (TiO_2) during the film preparation. In the sections below, the structure of the films were characterized by various spectral (IR, XRD, SEM-EDX and digital microscopy) and physicochemical characterization (TGA, pH dependence of the surface charge, solvent swelling, and water contact angle) methods. In turn, the composite films were evaluated for their photocatalytic efficacy of the neutralization of algal cells (*A. minutum*) in seawater to evaluate the potential of such materials for remediation of harmful algal blooms (HABs) in marine environments, as part of future studies in photocatalytic remediation to control HABs.

2.1. Characterization of the Fresh Hybrid Chitosan-Modified TiO_2 Films

2.1.1. Attenuated Total Reflectance Fourier Transformed Infrared Spectroscopy (ATR-FTIR) Analysis

The ATR-FTIR spectra of the films are shown in Figure 1a. Based on the FTIR spectrum of the chitosan film (Chi), the band at 1024 cm^{-1} corresponds to the symmetric stretching of the C–O–C bond. The band at 1072 cm^{-1} relates to the skeletal vibration of C–O and is usually assigned as the fingerprint band for the structure of chitosan [19]. The deformation vibration of –NH_2 is indicated by the appearance of an IR signature at 1554 cm^{-1}. The bands at 1384 cm^{-1} and 1317 cm^{-1} correspond to the asymmetric C–O–C stretching vibrations and C–O stretching vibration of CH–OH [20]. The band at 1645 cm^{-1} represents the C=O stretching of the amide group [21,22]. The small shoulder at 1151 cm^{-1} is due to the C–H vibration from C–O–C of chitosan.
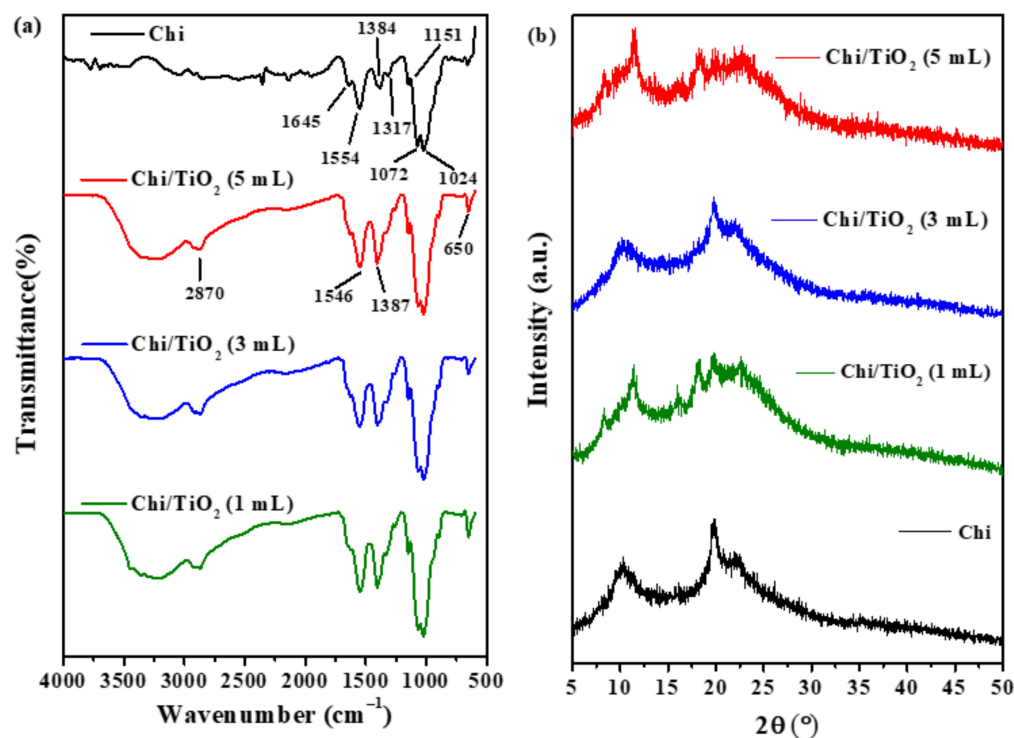

Figure 1. The (**a**) ATR-FTIR spectra and (**b**) XRD diffractograms of Chi and Chi/TiO_2 films.

The higher intensity of the IR band in the region of 3200–3500 cm^{-1} of chitosan/TiO_2 (Chi/TiO_2) films compared to Chi is due to the interaction between Ti with –OH and –NH functional groups of chitosan via hydrogen bonding [23]. The band formation at 2870 cm^{-1} was attributed to C–H asymmetric and symmetric vibrations of the Ti–OH

functional group [23]. The chemical reaction between the chitosan and TiO_2 is confirmed by the presence of an IR band at 1019 cm^{-1}, where this signature corresponds to the Ti–O–C bond [24,25]. The IR band associated with Ti–OH and Ti–O bonds can be seen at 1387 cm^{-1} [26], whereas the IR band related to the angular deformation of N–H bond of chitosan was observed at 1590 cm^{-1} [27]. The absorption at the lower frequency (650 cm^{-1}) is due to the symmetric stretching vibration of Ti–O–Ti and O–Ti–O flexion vibration of the anatase phase [28]. These bands support the presence of TiO_2 in the chitosan matrix.

In acidic media, the concentration of surface hydroxyl groups on the TiO_2 surface will be higher. These hydroxyl groups can react with those of chitosan via a condensation reaction to form Ti–O–C bonds. The cross-linking between the TiO_2 and the chitosan backbone is expected to reinforce the biopolymer and form a net-like structure that can capture and immobilize the algal cells. The presence of cross-linking is supported by the presence of an IR band at 1019 cm^{-1} for the Chi/TiO_2 films. The reaction scheme indicates an illustration of the cross-linking between the two groups, as shown in Scheme 1.
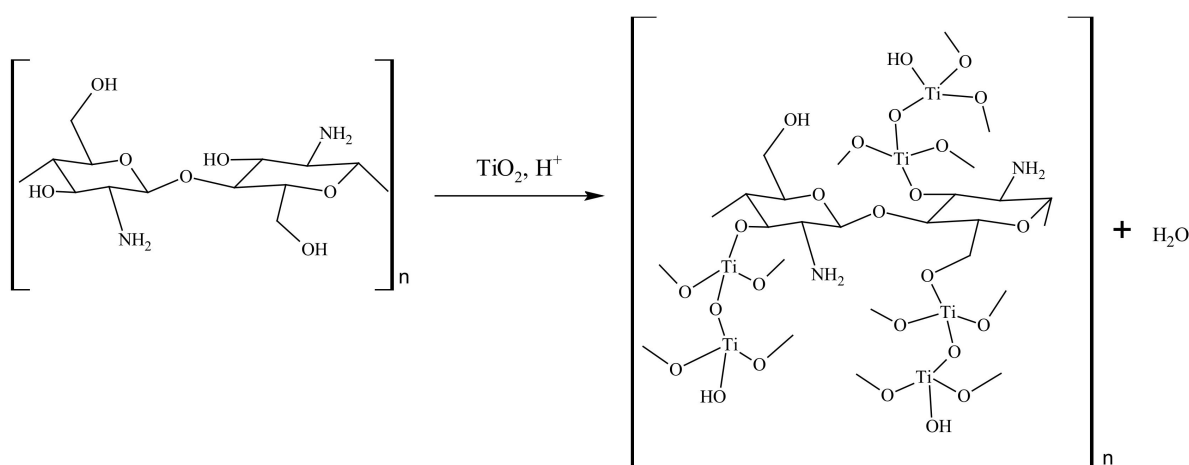
Scheme 1. The schematic representation showing the cross-linking between chitosan and TiO_2.

2.1.2. X-ray Diffraction (XRD) Analysis

The XRD profiles of Chi and the Chi/TiO_2 films are shown in Figure 1b. From the XRD diffractogram of Chi, three diffraction peaks can be observed at 2θ = 10.1°, 19.8° and 22° that correspond to the respective crystallographic planes of chitosan: (002), (101) and (220) [28,29].

The XRD peaks of chitosan became attenuated and broadened upon the incorporation of the TiO_2, which indicates a reduction in the crystallinity of chitosan and a decrease in the intermolecular hydrogen bonding of the chitosan matrix [28]. The characteristic peaks of anatase TiO_2 which occur at 2θ (°) values also correspond to the crystallographic planes denoted in parentheses: 25.42° (101), 38.08° (004), 38.93° (112), 48.35° (200), 63.02° (204), 69.17° (116), 70.62° (220), 75.43° (215) and 83.14° (224). The XRD lines of TiO_2 were not detected due to the low concentration of TiO_2 or uneven dispersion in the film matrix [30,31].

2.1.3. Scanning Electron Microscopy (SEM) Analysis

Figure 2 shows the SEM images for the surface morphology of the films (left side) and cross-sectioned images (right side). The formation of crater-like structures occurs due to the evaporation of water vapor and organic solvent during the film drying process. Meanwhile, the cross-section of Chi is observed to be dense and coarse but with no visible boundaries between chitosan and TiO_2 (Figure 2A,a). The surface of the Chi/TiO_2 films was observed to be different from Chi (Figure 2B–D). The surface of Chi/TiO_2 films was uneven and possibly due to the protrusion of irregularly shaped TiO_2 nanoparticles or due to the agglomeration of TiO_2 particles during the drying process. The cross-section

images of the Chi/TiO$_2$ films (Figure 2b–d) appear to be less coarse compared to Chi. The increase in the dosage of TiO$_2$ reduces the compact appearance of the films. Calero et al. have reported that a more compact structure is essential to enhance the film's capabilities for various applications [32].
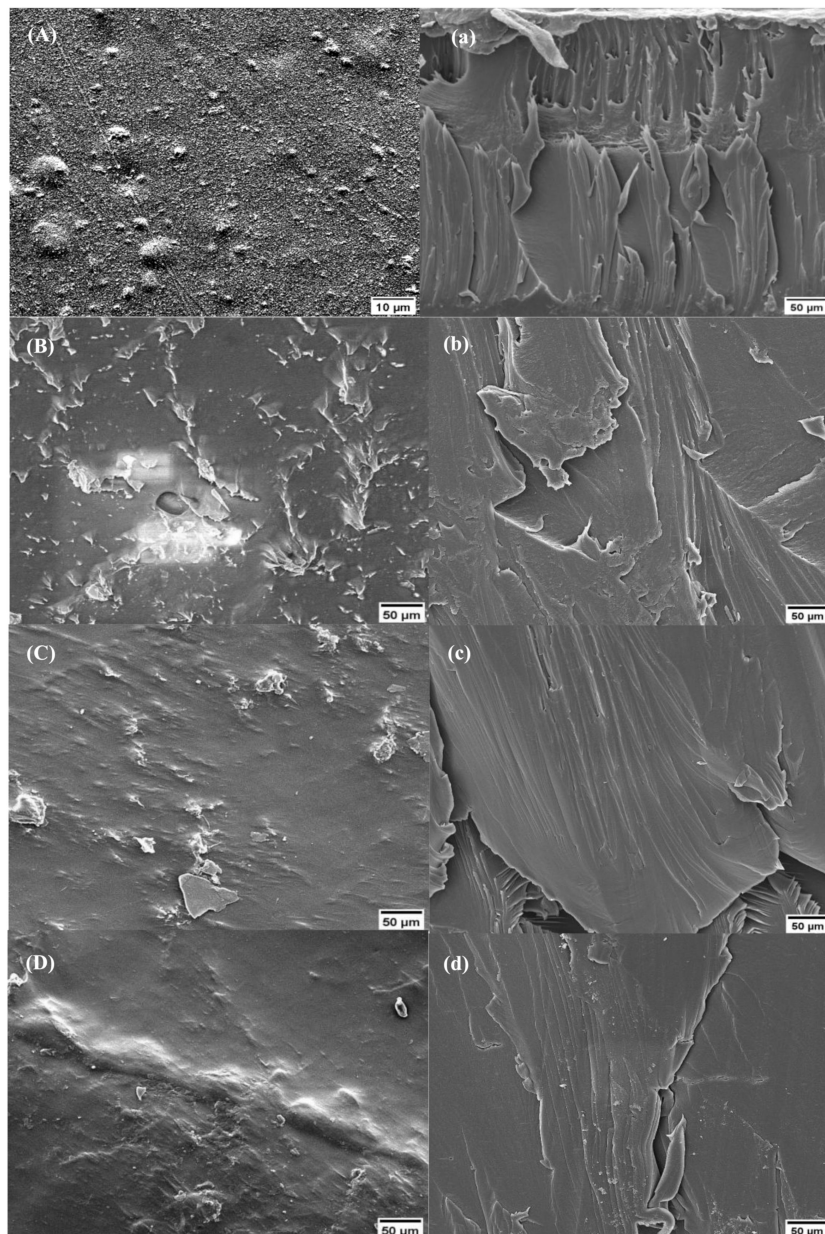
Figure 2. SEM images of surface and cross-sectional view of CH film (**A,a**); Chi/TiO$_2$ (1 mL) film (**B,b**); Chi/TiO$_2$ (3 mL) film (**C,c**); and Chi/TiO$_2$ (5 mL) (**D,d**) at 50 × magnification.

2.1.4. Point of Zero Charge (pH$_{pzc}$)

The point of zero charge (pH$_{pzc}$) is the pH value at which the surface of the solid is considered to have no net electrical charge [33]. The ability of any surface to adsorb ionic species of target pollutants is determined by the pH$_{pzc}$. The net surface charge on the particle is affected by the pH of the liquid media in which the solid is dispersed. The pH$_{pzc}$ determination of Chi and Chi/TiO$_2$ films is shown in Figure 3. The pH$_{pzc}$ of Chi/TiO$_2$ was lower compared to the pH$_{pzc}$ of a Chi film. The decrease indicates that TiO$_2$ altered the electronic structure and energy states of chitosan [34,35]. At a solution pH above the pH$_{pzc}$,

the surface of the films is negatively charged, whereas the surface becomes more positively charged at pH values below pH_{pzc}.
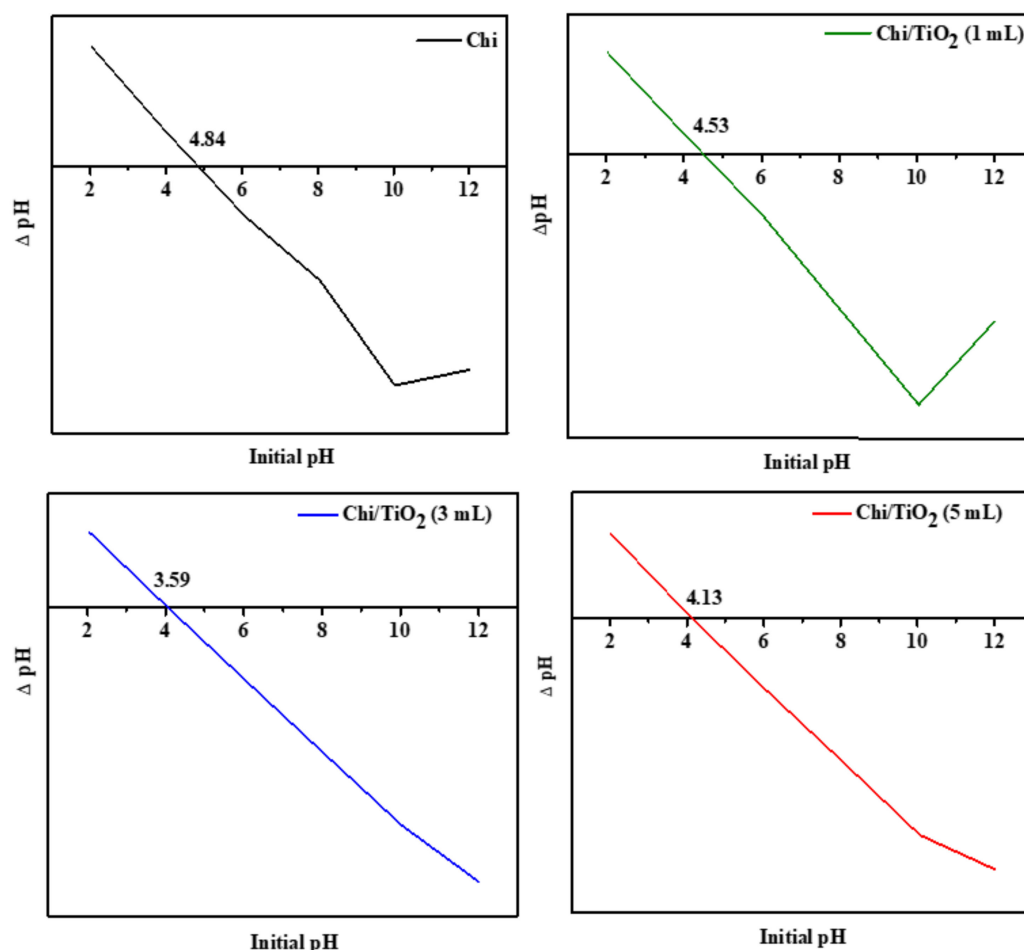

Figure 3. Graphs of Δ pH value were plotted against the pH_i to determine the intersection point at Δ pH zero of the films.

2.1.5. Wettability and Swelling Index Analysis

The hydrophilic or hydrophobic surface characteristics of the prepared films were established through a study of the variation in the water contact angle (θ) variation for films of variable composition. The θ-values for each film are presented in Table 1, where the highest θ-value is noted for the Chi film ($\theta = 98.2°$) due to the hydrophobic domains of the biopolymer [36]. The contact angle for the Chi film was observed to be similar to the reported values of chitosan films in the literature [37,38]. The θ-values of Chi/TiO$_2$ (1 mL and 5 mL) are slightly lower than Chi, whereas the Chi/TiO$_2$ (3 mL) shows the lowest contact angle (75.6°), which indicates a notable increase in the film hydrophilicity. The apparent increase for θ is due to the higher concentration of hydroxyl groups available to interact with water in the Chi/TiO$_2$ films, compared to a Chi film without TiO$_2$. The FTIR analysis indicates a greater level of hydroxyl groups in the Chi/TiO$_2$ films and none in the Chi film (Section 2.1.1). The lowest contact angle of Chi/TiO$_2$ (3 mL) may relate to the greater uniform distribution of TiO$_2$ nanoparticles compared to the other Chi/TiO$_2$ films. The even distribution of the TiO$_2$ increases the amount of hydrogen bond sites that may interact with water. The role of cross-linking may cause the microstructural surface heterogeneity or roughness of the film, which contribute to variable contact angle effects. From the SEM images (Section 2.1.3), it can be observed that Chi/TiO$_2$ (1 mL and 5 mL) appear uneven when compared to Chi/TiO$_2$ (3 mL). Greater surface heterogeneity or roughness can contribute to hydrophobic effects, which may inhibit the diffusion transport

of water molecules through the film [39]. Hence, the contact angle of Chi/TiO$_2$ (3 mL) film is lower than Chi/TiO$_2$ (1 mL and 5 mL) systems.

Table 1. The measured contact angle (θ) and swelling index of chitosan films.

Film Sample [1]	Swelling Index (%)	Contact Angle (θ; °)
Chi	63.7 ± 1.05	98.2 ± 0.84
Chi/TiO$_2$ (1 mL)	143.8 ± 2.67	93.0 ± 0.54
Chi/TiO$_2$ (3 mL)	150.7 ± 1.15	75.6 ± 0.03
Chi/TiO$_2$ (5 mL)	144.2 ± 1.09	92.8 ± 0.05

The values were expressed in mean ± standard deviation with a significant difference ($p < 0.05$); [1] The volume quantities in parentheses refer to the dosage of 0.2% *w/v* TiO$_2$.

The swelling index of the Chi/TiO$_2$ films was greater when compared to Chi films (without TiO$_2$), which is expected since both TiO$_2$ and Chi have hydrophilic properties. The TiO$_2$ is more likely to interact with the functional groups of chitosan such as –OH and –NH$_2$ which can likewise form hydrogen bonds with water molecules [40]. The functional groups increase the swelling of the film and also influence the hydrophilic character of the film [41,42]. The highest swelling index (%) of Chi/TiO$_2$ (3 mL) is due to its greater hydrophilic nature.

2.2. Photocatalytic Mitigation Studies

The removal efficiency (RE; %) values of the *A. minutum* sp. for Chi and Chi/TiO$_2$ films are shown in Figure 4. Based on the pH$_{pzc}$ of the films, the films will be negatively charged in seawater (pH = 6.8). Hence, the negatively charged algal cells will be repelled from the film surface. The slow swelling process of the film may also facilitate the trapping of algae cells in the net-like structure of the composite film to enable release and exchange with the external aqueous media. This is evident from the fluctuating RE values (%). The Chi, Chi/TiO$_2$ (3 mL) and Chi/TiO$_2$ (5 mL) films achieve ca. 20% removal of *A. minutum* at 72 h. Even though the swelling indices of the Chi/TiO$_2$ films were similar, Chi/TiO$_2$ (1 mL) has the lowest fluctuation and the highest RE (76.1 ± 13.8%). The lower RE value for Chi/TiO$_2$ (3 mL) may relate to its excessive swelling, which facilitates the release of the trapped algae to the aqueous media. The Chi/TiO$_2$ (3 mL) had the highest swelling index value. Whereas the lower RE value for Chi/TiO$_2$ (5 mL) was related to the agglomeration of TiO$_2$ nanoparticles, especially as the TiO$_2$ concentration was increased up to the highest level of film incorporation. Agglomeration and aggregation of the metal oxides such as TiO$_2$ were reported to affect the absorption of photons. In turn, a decrease in the ability to generate reactive oxygen species (ROS) such as the hydroxyl radical ($^\bullet$OH), which is responsible for the photodegradation of organic pollutants [43,44]. Since the agglomeration of TiO$_2$ in CH/TiO$_2$ (1 mL) is lower, more ROS can be generated to induce oxidative stress toward the algal cells. In turn, a greater production of ROS can cause organelle dysfunction, cell structure alteration and mutagenesis [45].

The mitigating ability of Chi/TiO$_2$ (1 mL) towards algal removal was compared to other semiconductor-based mitigating agents reported in the literature. Based on the results in Table 2, the RE value of Chi/TiO$_2$ (1 mL) is lower and relates to the high swelling rate of the film in seawater. In turn, the greater swelling contributes to the release of entrapped algae cells back to the surrounding aqueous environment. The intensity of the light source plays an important role in the generation of photogenerated electron/hole pairs. The intensity of the light used in this research was far lower (70 µmol photons m^{2}s^{-1}), based on the 16:8 h light: dark cycle, compared with the cited studies. The light intensity in this research might not be enough to generate higher levels of photogenerated electron/hole pairs. Hence, this effect may account for the lower overall RE values reported herein. Regardless, the current study showed that Chi/TiO$_2$ (1 mL) displayed better RE values under solar light irradiation. Future studies are planned where higher levels of solar

radiation will be used to study algal removal to better establish the deployment of this method for field-based applications.
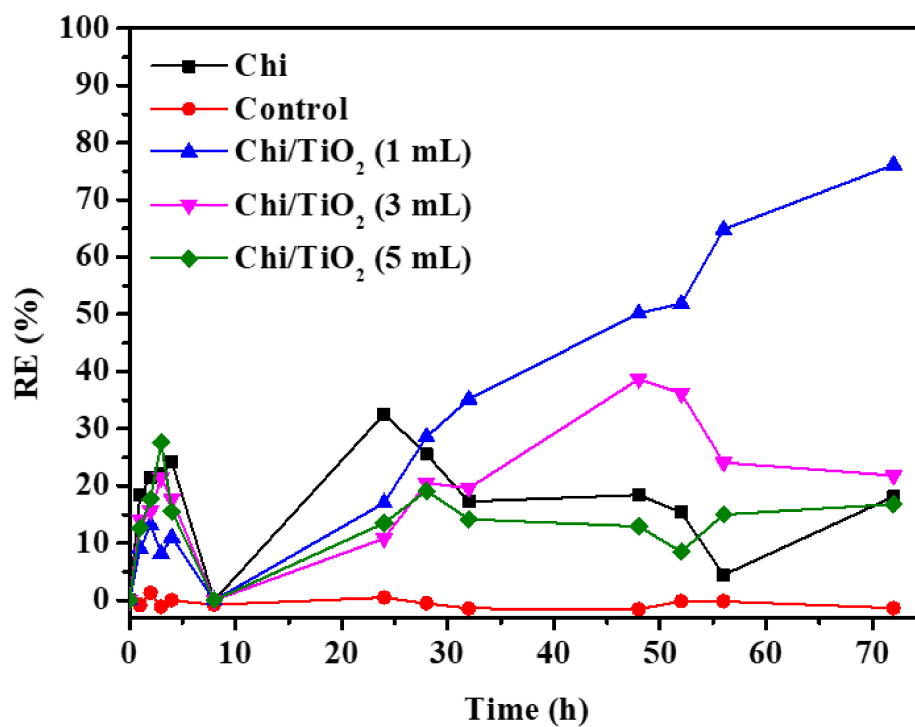

Figure 4. The RE values for various films: Chi film (control), Chi/TiO$_2$ (1 mL), Chi/TiO$_2$ (3 mL) and Chi/TiO$_2$ (5 mL) for 72 h.

Table 2. Removal efficiency of various HAB species using semiconductor-based mitigation agents, compared with Chi/TiO$_2$ (1 mL).

Mitigation Agent	HAB Species	Mitigation Approach	Removal Efficiency (%)	Lamp Intensity	Ref.
Fe$_2$O$_3$–TiO$_2$ NPs	*Chlorella vulgaris*	Chemical	High removal rate of algal cells (99.8%) within 24 h was achieved under visible light irradiation.	55 W/m^2	[9]
Ag/AgCl@ZIF-8 floating	*Chlorophyll a M. aeruginosa Other algae*	Physical	After 6 h of exposure to sunlight, the chlorophyll *a* degraded by 99.9%, *Microcystis aeruginosa* (92.6%) and biomass of the other algae decreased by about 80%.	Sunlight	[46]
Z-scheme g-C$_3$N$_4$-MoO$_3$ (Mo-CN) composite photocatalysts	*M. aeruginosa*	Chemical	15Mo-CN achieved a removal efficiency of 97% for the algal cells after 3 h of visible light irradiation.	48.1 W/m^2	[47]
γFe$_2$O$_3$/TiO$_2$ nanoparticle	*M. aeruginosa A. circinalis*	Physical	Within 1 h, *M. aerugonisa* (99.99%) and *A.cricinalis* (95.49) was removed.	32 W/m^2	[4]
Ag/AgCl@LaFeO$_3$ (ALFO) photocatalyst	*Phytoplankton*	Chemical	ALFO-20% had a higher photocatalytic activity with a near 100% removal rate of chlorophyll *a* within 150 min.	10,000 W/m^2	[48]
g-C$_3$N$_4$/Bi-TiO$_2$ floating photocatalyst	*M. aeruginosa*	Physical	Within 6 h of visible light illumination, 75.9% of *M. aeruginosa* was removed.	NA	[10]
Z-scheme Ag$_3$PO$_4$@PANI core–shell photocatalyst	*Microcystis aeruginosa*	Chemical	99.2% was *Microcystis aeruginosa* was removed within 3 h.	NA	[11]
SNP-TiO$_2$	*Karenia mikimotoi*	Chemical	Under visible light irradiation, 81.8% was removed within 96 h.	NA	[49]
ZnFe$_2$O$_4$/Ag$_3$PO$_4$/g-C$_3$N$_4$ (ZFO/AP/CN) photocatalyst	*M. aeruginosa* Microcystin-LR (MC-LR)	Physical	The photocatalytic removal of *M. aeruginosa* and MC-LR was 94.3% and 76.9%, respectively, under visible light.	NA	[11]
Floating BiOCl$_{0.6}$I$_{0.4}$/ZnO photocatalyst	*Microcystis aeruginosa*	Physical	The removal rate of chlorophyll *a* was 89.3% after 6 h of photocatalytic reaction under visible light.	42 W/m^2	[50]
Chi/TiO$_2$ (1 mL)	*Alexandrium minutum*	Physical	The removal of *Alexandrium minutum* was 76.1 ± 13.8% within 72 h.	70 μmol photons m^{2}s^{-1}	This study

2.3. Proposed Reaction Mechanism

One of the drawbacks of utilizing chitosan in seawater is the weakening of the netting and the bridging properties of the chitosan film, according to the high alkalinity and ionic strength of seawater [51,52]. Cross-linking of chitosan with TiO_2 will serve to strengthen its net-like structure for better adsorption of the algae cells. However, the adsorption of algae cells onto the films was limited due to repulsion forces between the negatively charged algae and the negatively charged film surface. Hence, it can be inferred that the mitigation process took place via a photocatalytic mechanism. The relationship between the conduction band (CB) and valence band (VB) potential of the TiO_2 was determined using Equation (1) to identify the ROS responsible for photocatalytic process.

$$E_{CB} = X - E^e - 0.5\, E_g \tag{1}$$

E_{CB} is the CB energy, X is the geometric mean of the electronegativity of the constituent atoms (5.82), E^e is the energy of a free electron on the hydrogen scale (approximately 4.5 eV) and E_g is the bandgap energy of the semiconductor (TiO_2 = 3.03 eV). The VB potential was determined through the following Equation (2).

$$E_{VB} = E_{CB} + E_g \tag{2}$$

The CB potential of the TiO_2 (−0.2 V) was determined to be less negative than $E°$ ($O_2/O_2^{\bullet-}$) = −0.33 V vs. NHE, indicating that the electrons produced in the reaction will not react with the adsorbed O_2 to produce $O_2^{\bullet-}$, which became channeled towards chitosan. The transfer of the photogenerated electrons to chitosan will prevent the electrons from combining with the holes. The VB potential of TiO_2 (2.38 V) was calculated to be higher than $E°$ ($^{\bullet}OH/OH^-$) = +1.99 V vs. NHE indicating that the photogenerated h^+ can oxidize OH^- into $^{\bullet}OH$. The generation of $^{\bullet}OH$ is simplified by the illustration in Figure 5.
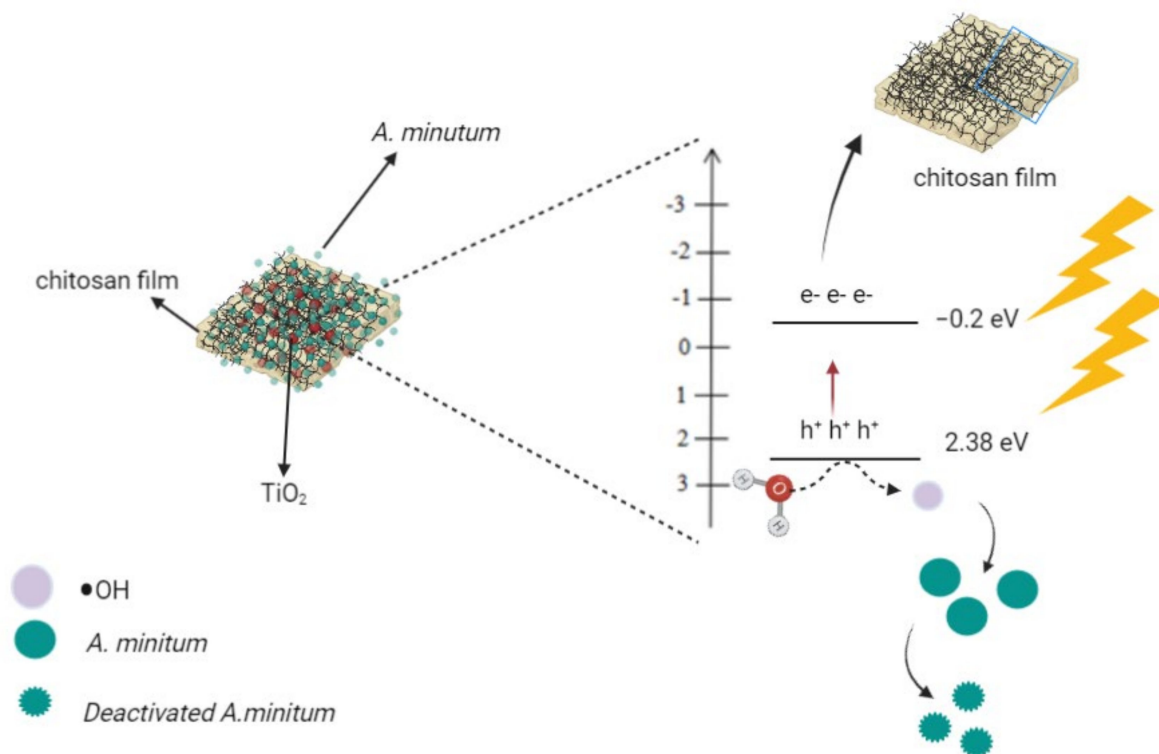

Figure 5. A proposed mechanism of $^{\bullet}OH$ generation by Chi/TiO_2 (1 mL) for the mitigation of *A. minutum*.

2.4. SEM and Digital Microscopy Analyses of the Films after Mitigation

The films after mitigation were subjected to SEM analysis to observe any structural changes of the films and the algae. As depicted in Figure 6a, the surface of the used Chi film became uneven with the appearance of distinctive hook-shaped particles which represent the apical pore complex of *A. minutum*. The surface of the Chi/TiO$_2$ films was constructed with irregularly shaped particles after the mitigation process, which may relate to the attachment of the algae cells (Figure 6b–d). This trend is in agreement with the SEM images before (Figure 2) and after (Figure 6) the photochemical treatment of the algae.
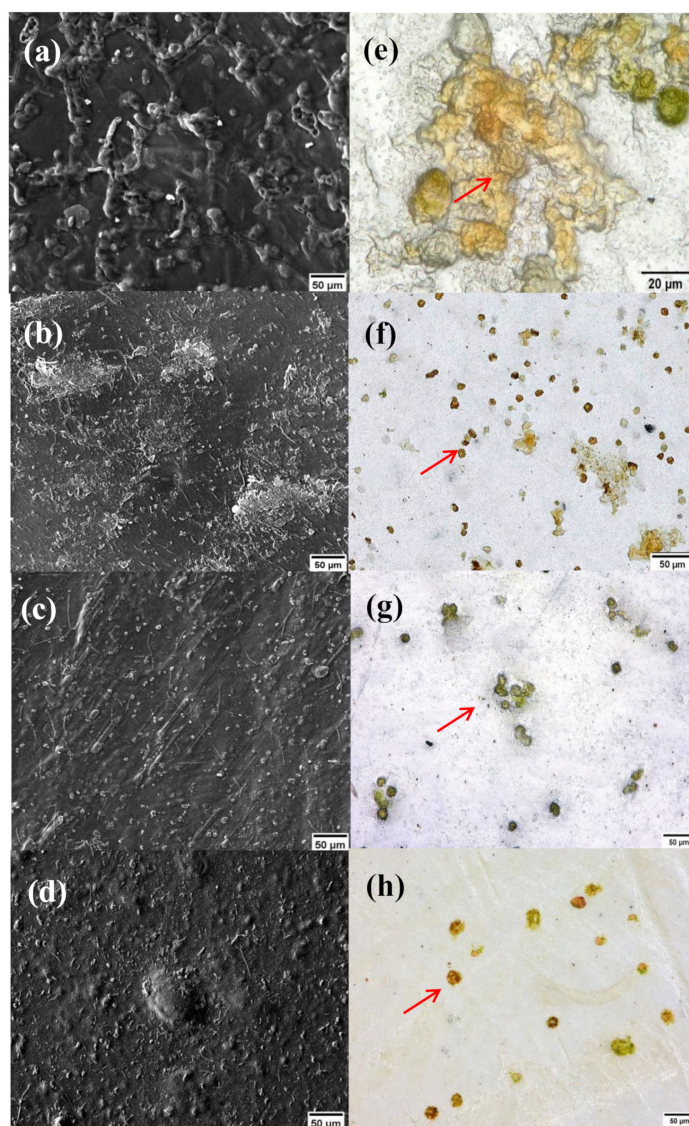

Figure 6. The SEM images (**a**) Chi, (**b**) Chi/TiO$_2$ (1 mL), (**c**) Chi/TiO$_2$ (3 mL) and (**d**) Chi/TiO$_2$ (5 mL); and digital microscopic images (**e**) Chi, (**f**) Chi/TiO$_2$ (1 mL), (**g**) Chi/TiO$_2$ (3 mL) and (**h**) Chi/TiO$_2$ (5 mL) after mitigation. The red arrows indicate the algal cell.

The used films were further analyzed using a digital microscope, where the corresponding images revealed that the algae cells attached to the Chi film were ruptured (shown in red arrow) (Figure 6e). The presence of positively charged amine groups of chitosan promote electrostatic interaction with the negatively charged algal cells, which contribute to cell rupture [53,54]. The algae cells in Figure 6f–h show that the cells were preserved after the mitigation process. The seawater systems have elevated ionic strength that hinders the unique surface characteristics of amorphous TiO$_2$, which prevents rupture

of the algae cells [55]. The absence of rupturing relates to charge screening effects due to the presence of sufficient ionic strength in the aqueous media.

2.5. Physical Appearance of Used Film Studies and Weight Change after Mitigation

The films were observed to undergo rupture and have a gel-like texture from absorbing the seawater during the mitigation studies. The weight of the dried use films decreased after mitigation suggesting that some of the films may have disintegrated during the process. The physical appearance of fresh and used films and their weight change after mitigation are given in Figure S1 and Table S1 (cf. Supplementary Materials).

3. Materials and Methods

3.1. Materials

Sodium hydroxide (NaOH) pellets (Qrec, 99%, Rawang, Malaysia), glacial acetic acid (Qrec, 100%, Rawang, Malaysia) and chitosan powder (Sigma-Aldrich, medium molecular weight, product id: 448877, St. Louis, MO, USA) were used without further purification. The anatase TiO_2 nanoparticle solution (0.2% *w/v*) was obtained from Prof. Ir. Dr. Srimala Sreekantan from the School of Materials & Mineral Resources, Engineering Campus, Universiti Sains Malaysia, Penang. The TiO_2 nanoparticles were prepared according to the method reported by N.H. Ahmad Barudin et al. [53], along with characterization of the physicochemical properties of the anatase TiO_2. The filtered seawater was supplied by Fisheries Research Institute (FRI), Batu Maung, Penang, Malaysia. The seawater pH before and after film immersion was recorded using a pH meter (Model Hanna edge^{pH}), where the seawater remained constant at pH~6.8.

3.2. Preparation of Hybrid Chitosan-Modified TiO_2 Film

A chitosan solution (2% *w/v*) was prepared by dissolving chitosan powder (2 g) in 100 mL of acetic acid solution (1% *v/v*). The solution was stirred for 4 h at 50 °C followed by centrifugation at 4000 rpm for 15 min. The solution was then filtered to remove any undissolved chitosan powder. Different dosages (1 mL, 3 mL and 5 mL) of 0.2% *w/v* of anatase TiO_2 were added into the chitosan solution and stirred for another 2 h to minimize the formation of bubbles and to form a homogeneous solution. The film-forming solution was then poured into a square-shaped Teflon mold, followed by oven-drying for 21 h at 50 °C. A NaOH solution (2% *w/v*) was prepared by dissolving 10.0 g of NaOH pellets in 500 mL distilled water. The dried film was soaked in 2% *w/v* NaOH aqueous solution for a minute and then rinsed with distilled water to neutralize it. The film was then dried at room temperature for 24 h and kept in a desiccator for further use. The films were labelled as Chi (chitosan film) and Chi/TiO_2 (*x* mL; *x* = 1, 3 and 5 mL)

3.3. Characterization

3.3.1. Attenuated Total Reflectance Fourier Transform Infrared (ATR-FTIR) Spectroscopy

The ATR-FTIR spectrophotometer (Perkin Elmer FT-NIR spectrometer with Universal ATR sampling accessory, Waltham, MA, USA) was used to identify the film's functional groups. The spectra of the films were analyzed over the spectral range of 4000 to 600 cm^{-1} with 64 scans.

3.3.2. Scanning Electron Microscopy with Energy Dispersive X-ray (SEM-EDX)

The surface topology, cross-section and elemental composition of the films were analyzed using SEM-EDX analysis (SEM Leica Cambridge S360-EDX Falcon System, Cambridge, UK). The films were cut into 1 cm × 1 cm prior to being fixed onto a stub containing carbon adhesive and sputtered with gold for 10–15 min in an airtight sputter coater (Armetech, Ozolnieki, Latvia) to sharpen the SEM images.

3.3.3. Thermogravimetric Analysis (TGA)

The changes in the mass of the films in relation to the changes in temperature were determined using a TGA analyzer (Perkin Elmer). Approximately 6 mg of the films was heated from 30 to 600 °C at 10 °C min^{-1} under a nitrogen flow (50 cm^3/min).

3.3.4. X-ray Diffraction (XRD)

A Bruker-D8 Advance Powder X-ray diffraction (XRD) (Billerica, MA, USA) was used to determine the crystalline phases and the degree of crystallinity of the films. The diffractogram was obtained for each film at 2θ angle of 5° to 50°. The diffractometer was equipped with CuKα radiation, λ = 0.1541 nm, voltage = 40 kV and current = 30 mA.

3.3.5. Swelling Index (SI)

The swelling index (SI) of the films was estimated by submerging the pre-weighed dry films into 100 mL of seawater for 24 h at room temperature. After 24 h, the swollen films were removed, wiped with filter paper to remove residual excess water and then weighed. The SI was calculated using Equation (3) as reported by Sabzevari et al. [54]. Three films were tested at each film composition to obtain the average swelling index.

$$SI\ (\%) = \frac{(W_f - W_i)}{W_i} \times 100 \tag{3}$$

W_f is the weight of the swollen film after 24 h and W_i is the weight of dry film before being submerged in the aqueous media.

3.3.6. Wettability Test (WS)

The film's wettability or water contact angle (CA) was tested via the static CA using a goniometer (Ramé-Hart Instrument Co., Succasunna, NJ, USA) based on the Sessile drop method. Deionized water (4 μL) was dropped using a microsyringe onto the smooth surface of the film at room temperature. Then, a microscope was used to capture the micrograph images. This step was repeated for five different spots of the membrane sample to calculate the average CA.

3.3.7. Point of Zero Charge (pzc)

The surface charge of the films was performed using the reported method by Shah et al. with some modification [33].Firstly, 100 mL of distilled water was poured into six 200 mL beakers. The initial pH of the distilled water (pH$_i$) was adjusted from pH 2 to 12 using 0.1 M HCl and/or 0.1 M NaOH solution. Then, the film was submerged into each beaker and shaken for 24 h at a shaking rate of 250 rpm. The final pH of the distilled water (pH$_f$) was recorded. The difference in pH values (Δ pH) was calculated using Equation (4):

$$\Delta\,pH\ =\ pH_f -\ pH_i \tag{4}$$

Finally, the Δ pH value was plotted against the pH$_i$ to determine the intersection point at Δ pH zero to estimate the pzc. This pH indicates the surface charge density of the film.

3.3.8. Mitigation of Alexandrium Minutum

A. minutum cells were grown in ES-Dk medium at 25 °C under a light intensity of 70 μmol photons m^{2}s^{-1} using a 16:8 h (light:dark) photocycle [55]. Filtered natural seawater diluted to 15 ppt was used as solution medium for *A. minutum* culture. The cell removal experiments were performed when the culture reached the exponential growth phase. Cultures of *A. minutum* with a cell concentration of 2×10^4 cell/mL were used for the experiments.

The mitigation of *A.minutum* was carried out via physical method in a 250 mL beaker that contained 100 mL of the cell culture that was placed on a table in a static condition. The film was hung so that $\frac{3}{4}$ of its dimension was submerged into the reaction medium.

Approximately 1 mL of the sample from 2 cm below the solution surface was collected and preserved with one drop of Lugol's solution at each specific time interval. The preserved cells were counted using the Sedgewick-rafter counter under a light microscope (Leica CME, Wetzlar, Germany) at 10× magnification. The change in the structure of the cells on the surface of the films was observed under the digital microscope (Keyence VHX E-100, Osaka, Japan). The removal efficiency (RE) was calculated using Equation (5) [56]. All the RE data were expressed as the mean ± standard deviation (S.D.).

$$RE\ (\%) = 1 - \left[\frac{\text{Final cell concentration in sample}}{\text{Final cell concentration in control}} \right] \times 100 \tag{5}$$

Upon completion of the mitigation process, the films were separated for further characterization using SEM and a digital microscope.

3.3.9. Statistical Analysis

The statistical analysis was performed using GraphPad Prism 5 version 5.01. The obtained data were expressed as the mean ± standard deviation of the triplicate measurements. The distinction between the experimental groups was evaluated using a one-way variance (ANOVA) analysis. A *p*-value less or equal to 0.05 was estimated to be statistically significant.

4. Conclusions

Hybrid chitosan-modified TiO_2 thin films (CH/TiO_2 (*x* mL; *x* = 1, 3 and 5 mL)) were successfully synthesized via solvent casting method for the mitigation of *A.minutum* in a lab-scale experimental setup. The negatively charged surface of the films repelled the negatively charged algae cells and caused the RE values (%) to fluctuate. The CH/TiO_2 (1 mL) was able to remove 76.1 ± 13.8% of algae cells within 72 h due to its ability to generate hydroxyl radicals which can cause oxidative stress to the adsorbed and free algae. The results obtained from this study showed that the hybrid chitosan-modified TiO_2 film can be used to mitigate harmful algal blooms. In particular, future studies are planned to study the effect of higher levels of solar radiation on the efficacy of algal removal in order to establish this method for field-based applications. Further studies are also required to determine the suitability of this mitigation method in marine-based environments to determine the effect of such materials towards other marine biota.

References

1. Anderson, D.M. Approaches to Monitoring, Control and Management of Harmful Algal Blooms (HABs). *Ocean. Coast. Manag.* **2009**, *52*, 342–347. [CrossRef] [PubMed]

2. Havens, K.E.; Paerl, H.W. Climate Change at a Crossroad for Control of Harmful Algal Blooms. *Environ. Sci. Technol.* **2015**, *49*, 12605–12606. [CrossRef] [PubMed]

3. Shriwastav, A.; Thomas, J.; Bose, P. A Comprehensive Mechanistic Model for Simulating Algal Growth Dynamics in Photobioreactors. *Bioresour. Technol.* **2017**, *233*, 7–14. [CrossRef] [PubMed]

4. Madany, P.; Xia, C.; Bhattacharjee, L.; Khan, N.; Li, R.; Liu, J. Antibacterial Activity of Fe_2O_3 /TiO_2 Nanoparticles on Toxic Cyanobacteria from a Lake in Southern Illinois. *Water Environ. Res.* **2021**, *93*, 2807–2818. [CrossRef]

5. Berdalet, E.; Fleming, L.E.; Gowen, R.; Davidson, K.; Hess, P.; Backer, L.C.; Moore, S.K.; Hoagland, P.; Enevoldsen, H. Marine Harmful Algal Blooms, Human Health and Wellbeing: Challenges and Opportunities in the 21st Century. *J. Mar. Biol. Ass.* **2016**, *96*, 61–91. [CrossRef]

6. Iqbal, A.; Ahmad, N.; Mohammad Noor, N.; Wilson, L.D.; Ibrahim, N.H. Mitigation of Toxic *Alexandrium Tamiyavanichii* Using Chitosan-Silica Composite. *Malays. J. Anal. Sci.* **2019**, *23*, 31–39. [CrossRef]

7. Hasija, V.; Raizada, P.; Sudhaik, A.; Sharma, K.; Kumar, A.; Singh, P.; Jonnalagadda, S.B.; Thakur, V.K. Recent Advances in Noble Metal Free Doped Graphitic Carbon Nitride Based Nanohybrids for Photocatalysis of Organic Contaminants in Water: A Review. *Appl. Mater. Today* **2019**, *15*, 494–524. [CrossRef]

8. Rezayian, M.; Niknam, V.; Ebrahimzadeh, H. Oxidative Damage and Antioxidative System in Algae. *Toxicol. Rep.* **2019**, *6*, 1309–1313. [CrossRef]

9. Baniamerian, H.; Tsapekos, P.; Alvarado-Morales, M.; Shokrollahzadeh, S.; Safavi, M.; Angelidaki, I. Anti-Algal Activity of Fe_2O_3–TiO_2 Photocatalyst on *Chlorella Vulgaris* Species under Visible Light Irradiation. *Chemosphere* **2020**, *242*, 125119. [CrossRef]

10. Song, J.; Li, C.; Wang, X.; Zhi, S.; Wang, X.; Sun, J. Visible-Light-Driven Heterostructured g-C_3N_4/Bi-TiO_2 Floating Photocatalyst with Enhanced Charge Carrier Separation for Photocatalytic Inactivation of *Microcystis aeruginosa*. *Front. Environ. Sci. Eng.* **2021**, *15*, 129. [CrossRef]

11. Fan, G.; Lin, X.; You, Y.; Du, B.; Li, X.; Luo, J. Magnetically Separable $ZnFe_2O_4$/Ag_3PO_4/g-C_3N_4 Photocatalyst for Inactivation of *Microcystis aeruginosa*: Characterization, Performance and Mechanism. *J. Hazard. Mater.* **2022**, *421*, 126703. [CrossRef]

12. Aranaz, I.; Alcántara, A.R.; Civera, M.C.; Arias, C.; Elorza, B.; Heras Caballero, A.; Acosta, N. Chitosan: An Overview of Its Properties and Applications. *Polymers* **2021**, *13*, 3256. [CrossRef]

13. Kazachenko, A.S.; Akman, F.; Malyar, Y.N.; Issaoui, N.; Vasilieva, N.Y.; Karacharov, A.A. Synthesis Optimization, DFT and Physicochemical Study of Chitosan Sulfates. *J. Mol. Struct.* **2021**, *1245*, 131083. [CrossRef]

14. Razzaz, A.; Ghorban, S.; Hosayni, L.; Irani, M.; Aliabadi, M. Chitosan Nanofibers Functionalized by TiO_2 Nanoparticles for the Removal of Heavy Metal Ions. *J. Taiwan Inst. Chem. Eng.* **2016**, *58*, 333–343. [CrossRef]

15. Saravanan, R.; Aviles, J.; Gracia, F.; Mosquera, E.; Gupta, V.K. Crystallinity and Lowering Band Gap Induced Visible Light Photocatalytic Activity of TiO_2/CS (Chitosan) Nanocomposites. *Int. J. Biol. Macromol.* **2018**, *109*, 1239–1245. [CrossRef]

16. Zhao, Y.; Tao, C.; Xiao, G.; Su, H. Controlled Synthesis and Wastewater Treatment of Ag_2O/TiO_2 Modified Chitosan-Based Photocatalytic Film. *RSC Adv.* **2017**, *7*, 11211–11221. [CrossRef]

17. Abdullah Al Balushi, K.S.; Devi, G.; Saif Al Hudaifi, A.; Khamis Al Garibi, A.S.R. Development of Chitosan-TiO_2 Thin Film and Its Application for Methylene Blue Dye Degradation. *Int. J. Environ. Anal. Chem.* **2021**, 1–14. [CrossRef]

18. Usup, G.; Pin, L.C.; Ahmad, A.; Teen, L.P. *Alexandrium* (Dinophyceae) Species in Malaysian Waters. *Harmful Algae* **2002**, *1*, 265–275. [CrossRef]

19. Mahatmanti, F.W.; Nuryono, N.; Narsito, N. Physical Characteristics of Chitosan Based Film Modified with Silica and Polyethylene Glycol. *Indones. J. Chem.* **2014**, *14*, 131–137. [CrossRef]

20. Budnyak, T.M.; Pylypchuk, I.V.; Tertykh, V.A.; Yanovska, E.S.; Kolodynska, D. Synthesis and Adsorption Properties of Chitosan-Silica Nanocomposite Prepared by Sol-Gel Method. *Nanoscale Res. Lett.* **2015**, *10*, 87. [CrossRef]

21. Wan, Y.; Wu, H.; Yu, A.; Wen, D. Biodegradable Polylactide/Chitosan Blend Membranes. *Biomacromolecules* **2006**, *7*, 1362–1372. [CrossRef]

22. Duan, B.; Dong, C.; Yuan, X.; Yao, K. Electrospinning of Chitosan Solutions in Acetic Acid with Poly(Ethylene Oxide). *J. Biomater. Sci. Polym. Ed* **2004**, *15*, 797–811. [CrossRef] [PubMed]

23. Lin, B.; Luo, Y.; Teng, Z.; Zhang, B.; Zhou, B.; Wang, Q. Development of Silver/Titanium Dioxide/Chitosan Adipate Nanocomposite as an Antibacterial Coating for Fruit Storage. *LWT Food Sci. Technol.* **2015**, *63*, 1206–1213. [CrossRef]

24. Zhu, X.; Chang, Y.; Chen, Y. Toxicity and Bioaccumulation of TiO_2 Nanoparticle Aggregates in *Daphnia magna*. *Chemosphere* **2010**, *78*, 209–215. [CrossRef]

25. Farzana, M.H.; Meenakshi, S. Photo-Decolorization and Detoxification of Toxic Dyes Using Titanium Dioxide Impregnated Chitosan Beads. *Int. J. Biol. Macromol.* **2014**, *70*, 420–426. [CrossRef]

26. Díaz-Visurraga, J.; Gutiérrez, C.; von Plessing, C.; García, A. Metal Nanostructures as Antibacterial Agents. In *Science And Technology Against Microbial Pathogens: Research, Development and Evaluation*; Méndez-Vilas, A., Ed.; Formatex: Badajoz, Spain, 2011.

27. Wiącek, A.E.; Gozdecka, A.; Jurak, M. Physicochemical Characteristics of Chitosan–TiO_2 Biomaterial. 1. Stability and Swelling Properties. *Ind. Eng. Chem. Res.* **2018**, *57*, 1859–1870. [CrossRef]

28. Al-Taweel, S.S.; Saud, R.H. New Route for Synthesis of Pure Anatase TiO$_2$ Nanoparticles via Utrasound-assisted Sol-Gel Method. *J. Chem. Pharm. Res.* **2016**, *8*, 620–626.

29. Khan, A.; Khan, R.A.; Salmieri, S.; Le Tien, C.; Riedl, B.; Bouchard, J.; Chauve, G.; Tan, V.; Kamal, M.R.; Lacroix, M. Mechanical and Barrier Properties of Nanocrystalline Cellulose Reinforced Chitosan Based Nanocomposite Films. *Carbohydr. Polym.* **2012**, *90*, 1601–1608. [CrossRef]

30. Theivasanthi, T.; Alagar, M. Titanium Dioxide (TiO$_2$) Nanoparticles XRD Analyses: An Insight. *arXiv* **2013**, arXiv:1307.1091. [CrossRef]

31. Xing, Y.; Li, X.; Guo, X.; Li, W.; Chen, J.; Liu, Q.; Xu, Q.; Wang, Q.; Yang, H.; Shui, Y.; et al. Effects of Different TiO$_2$ Nanoparticles Concentrations on the Physical and Antibacterial Activities of Chitosan-Based Coating Film. *Nanomaterials* **2020**, *10*, 1365. [CrossRef]

32. López Calero, J.; Oquendo Berríos, Z.; Suarez, O.M. Biodegradable Chitosan Matrix Composite Reinforced with Titanium Dioxide for Biocidal Applications. In *Renewable and Sustainable Composites*; Pereira, A.B., Fernandes, F.A.O., Eds.; IntechOpen: London, UK, 2019. [CrossRef]

33. Shah, I.; Adnan, R.; Wan Ngah, W.S.; Mohamed, N. Iron Impregnated Activated Carbon as an Efficient Adsorbent for the Removal of Methylene Blue: Regeneration and Kinetics Studies. *PLoS ONE* **2015**, *10*, e0122603. [CrossRef] [PubMed]

34. Abdullah, O.G.; Aziz, S.B.; Omer, K.M.; Salih, Y.M. Reducing the Optical Band Gap of Polyvinyl Alcohol (PVA) Based Nanocomposite. *J. Mater. Sci. Mater. Electron.* **2015**, *26*, 5303–5309. [CrossRef]

35. Taspika, M.; Desiati, R.D.; Mahardika, M.; Sugiarti, E.; Abral, H. Influence of TiO$_2$/Ag Particles on the Properties of Chitosan Film. *Adv. Nat. Sci. Nanosci. Nanotechnol.* **2020**, *11*, 015017. [CrossRef]

36. Almeida, E.V.R.; Frollini, E.; Castellan, A.; Coma, V. Chitosan, Sisal Cellulose, and Biocomposite Chitosan/Sisal Cellulose Films Prepared from Thiourea/NaOH Aqueous Solution. *Carbohydr. Polym.* **2010**, *80*, 655–664. [CrossRef]

37. Zhang, X.; Xiao, G.; Wang, Y.; Zhao, Y.; Su, H.; Tan, T. Preparation of Chitosan-TiO$_2$ Composite Film with Efficient Antimicrobial Activities under Visible Light for Food Packaging Applications. *Carbohydr. Polym.* **2017**, *169*, 101–107. [CrossRef]

38. Luo, Y.; Pan, X.; Ling, Y.; Wang, X.; Sun, R. Facile Fabrication of Chitosan Active Film with Xylan via Direct Immersion. *Cellulose* **2014**, *21*, 1873–1883. [CrossRef]

39. Liu, H.; Adhikari, R.; Guo, Q.; Adhikari, B. Preparation and Characterization of Glycerol Plasticized (High-Amylose) Starch–Chitosan Films. *J. Food Eng.* **2013**, *116*, 588–597. [CrossRef]

40. Clasen, C.; Wilhelms, T.; Kulicke, W.-M. Formation and Characterization of Chitosan Membranes. *Biomacromolecules* **2006**, *7*, 3210–3222. [CrossRef]

41. Huang, L.; Dai, T.; Xuan, Y.; Tegos, G.P.; Hamblin, M.R. Synergistic Combination of Chitosan Acetate with Nanoparticle Silver as a Topical Antimicrobial: Efficacy against Bacterial Burn Infections. *Antimicrob. Agents Chemother.* **2011**, *55*, 3432–3438. [CrossRef]

42. Palla-Rubio, B.; Araújo-Gomes, N.; Fernández-Gutiérrez, M.; Rojo, L.; Suay, J.; Gurruchaga, M.; Goñi, I. Synthesis and Characterization of Silica-Chitosan Hybrid Materials as Antibacterial Coatings for Titanium Implants. *Carbohydr. Polym.* **2019**, *203*, 331–341. [CrossRef]

43. Jassby, D.; Farner Budarz, J.; Wiesner, M. Impact of Aggregate Size and Structure on the Photocatalytic Properties of TiO$_2$ and ZnO Nanoparticles. *Environ. Sci. Technol.* **2012**, *46*, 6934–6941. [CrossRef]

44. Pellegrino, F.; Pellutiè, L.; Sordello, F.; Minero, C.; Ortel, E.; Hodoroaba, V.-D.; Maurino, V. Influence of Agglomeration and Aggregation on the Photocatalytic Activity of TiO$_2$ Nanoparticles. *Appl. Catal. B* **2017**, *216*, 80–87. [CrossRef]

45. Juan, C.A.; Pérez de la Lastra, J.M.; Plou, F.J.; Pérez-Lebeña, E. The Chemistry of Reactive Oxygen Species (ROS) Revisited: Outlining Their Role in Biological Macromolecules (DNA, Lipids and Proteins) and Induced Pathologies. *Int. J. Mol. Sci.* **2021**, *22*, 4642. [CrossRef]

46. Fan, G.; Chen, Z.; Wang, B.; Wu, S.; Luo, J.; Zheng, X.; Zhan, J.; You, Y.; Zhang, Z. Photocatalytic Removal of Harmful Algae in Natural Waters by Ag/AgCl@ZIF-8 Coating under Sunlight. *Catalysts* **2019**, *9*, 698. [CrossRef]

47. Wang, D.; Ao, Y.; Wang, P. Effective Inactivation of *Microcystis aeruginosa* by a Novel Z-Scheme Composite Photocatalyst under Visible Light Irradiation. *Sci. Total Environ.* **2020**, *746*, 141149. [CrossRef]

48. Fan, G.; Chen, Z.; Yan, Z.; Du, B.; Pang, H.; Tang, D.; Luo, J.; Lin, J. Efficient Integration of Plasmonic Ag/AgCl with Perovskite-Type LaFeO$_3$: Enhanced Visible-Light Photocatalytic Activity for Removal of Harmful Algae. *J. Hazard. Mater.* **2021**, *409*, 125018. [CrossRef]

49. Hu, L.; Wang, R.; Wang, M.; Wang, C.; Xu, Y.; Wang, Y.; Gao, P.; Liu, C.; Song, Y.; Ding, N.; et al. The Inactivation Effects and Mechanisms of Karenia Mikimotoi by Non-Metallic Elements Modified TiO$_2$ (SNP-TiO$_2$) under Visible Light. *Sci. Total Environ.* **2022**, *820*, 153346. [CrossRef]

50. Liu, H.; Yang, L.; Chen, H.; Chen, M.; Zhang, P.; Ding, N. Preparation of Floating BiOCl$_{0.6}$I$_{0.4}$/ZnO Photocatalyst and Its Inactivation of *Microcystis aeruginosa* under Visible Light. *J. Environ. Sci.* **2023**, *125*, 362–375. [CrossRef]

51. Qun, G.; Ajun, W. Effects of Molecular Weight, Degree of Acetylation and Ionic Strength on Surface Tension of Chitosan in Dilute Solution. *Carbohydr. Polym.* **2006**, *64*, 29–36. [CrossRef]

52. Bhalkaran, S.; Wilson, L. Investigation of Self-Assembly Processes for Chitosan-Based Coagulant-Flocculant Systems: A Mini-Review. *IJMS* **2016**, *17*, 1662. [CrossRef]

53. Ahmad Barudin, N.H.; Sreekantan, S.; Ong, M.T.; Lai, C.W. Synthesis, Characterization and Comparative Study of Nano-Ag–TiO$_2$ against Gram-Positive and Gram-Negative Bacteria under Fluorescent Light. *Food Control* **2014**, *46*, 480–487. [CrossRef]

54. Sabzevari, M.; Cree, D.E.; Wilson, L.D. Mechanical Properties of Graphene Oxide-Based Composite Layered-Materials. *Mater. Chem. Phys.* **2019**, *234*, 81–89. [CrossRef]

55. Kokinos, J.P.; Anderson, D.M. Morphological Development of Resting Cysts in Cultures of the Marine Dinoflagellate *Lingulodinium polyedrum* (= *L. machaerophorum*). *Palynology* **1995**, *19*, 143–166. [CrossRef]

56. Kim, Z.-H.; Thanh, N.N.; Yang, J.-H.; Park, H.; Yoon, M.-Y.; Park, J.-K.; Lee, C.-G. Improving Microalgae Removal Efficiency Using Chemically-Processed Clays. *Biotechnol. Bioproc. E* **2016**, *21*, 787–793. [CrossRef]